Available online at www.sciencedirect.com
SCIENCE DIRECT®

Journal of the European Ceramic Society 23 (2003) 1649–1654
www.elsevier.com/locate/jeurceramsoc

Preparation of machinable Ce–TZP/$CePO_4$ composite ceramics by liquid precursor infiltration

Zhenjun Zhou, Wei Pan, Zhipeng Xie*

State Key Lab of New Ceramics and Fine Processing, Department of Materials Science and Engineering, Tsinghua University, Beijing 100082, People's Republic of China

Received 14 June 2001; accepted 5 October 2002

Abstract

A novel process has been used to fabricate Ce–TZP/$CePO_4$ composite ceramics: namely infiltrating $CePO_4$ liquid precursor into Ce–TZP porous ceramic. Sintered Ce–TZP ceramic preform with 35 vol.% open pore volume was developed by adding graphite 30 vol.%. The Ce–TZP/$CePO_4$ composite ceramics containing different $CePO_4$ contents were obtained by infiltration and pyrolysis cycles. The machinability and mechanical properties of these materials were investigated. Results show that the Ce–TZP/$CePO_4$ composite ceramics can be cut and drilled using conventional tungsten carbide metal-working tools. Measurement of normal grinding force was used to compare the ease of machining in these materials. The machinable Ce–TZP/$CePO_4$ composites containing a range from 2.3 to 7.5 vol.% $CePO_4$ has good machinability as well as maintaining outstanding mechanical properties. The relation between microstructure and mechanical properties of the materials was discussed.

Keywords: ZrO_2; $CePO_4$; Mechanical properties; Microstructure; Liquid infiltration

1. Introduction

Ceramic materials have been used as engineering materials because of their high strength and high hardness. One significant disadvantage of such ceramics was their difficulty in machining after sintering, which led to high machining cost. To decrease it, various ceramics with machinability, called machinable ceramics, have been developed. Machinable glass-ceramic, consisting of finely dispersed mica platelets in a glass matrix, could be cut and drilled by using conventional metal-work tools.[1] The ease of cutting derived from cleavage of the mica crystal beneath the cutting tool, and material removal by linking of microcracks. Attempts have been made to develop analogous, more refractory systems. Barsoum et al.[2] showed that Ti_3SiC_2, consisting of large, plate-shaped, easily cleaved grains, could be drilled and tapped using high-speed steel tools. Padture et al.[3] showed that material removal rates during grinding and drilling of silicon carbide could be substantially increased by incorporating elongated grains, weak interphase boundaries, and high internal stresses into the microstructure. The microstructure consisted of plate-shape SiC grains with a second phase of yttrium aluminum garnet with relatively weak interphase bonding. Kawai et al.[4] showed that silicon nitride (Si_3N_4) containing porosity was machinable. Davis et al.[5] reported on another class of machinable ceramics, based on two-phase mixtures of refractory oxide (e.g. Al_2O_3, ZrO_2, mullite) and rare-earth phosphates (e.g. $CePO_4$, $LaPO_4$). The bonding between the two phases is weak. Zirconia can be rendered "machinable" by the addition of finely dispersed rare-earth phosphate, in an amount at least as small as 20 vol.%. The ease of diamond grinding was increased in the case of zirconia by the addition of $CePO_4$, but the relative change was much smaller. Moreover, the mechanical properties of zirconia containing high $CePO_4$ had a serious degradation.

In this paper, The fabrication and preliminary testing of machinable Ce–TZP/$CePO_4$ composite ceramics are reported. Based on the advanced design and sophisticated technology of the ceramic, the combination of Ce–TZP and $CePO_4$ would effectively improve the Ce–TZP ceramics' machinability as well as maintaining outstanding mechanical properties.

* Corresponding author.
E-mail address: zhenjunzhou@eyou.com (Z. Xie).

0955-2219/03/$ - see front matter
PII: S0955-2219(02)00368-0

2. Experimental procedure

Flow chart for the preparation of the machinable Ce–TZP/$CePO_4$ composite ceramics is shown in Fig. 1. The porous zirconia was fabricated using colloidal consolidation and presintering. In the first stage, the zirconia ceramic powder (12 mol%-CeO_2-doped ZrO_2, average particle size 0.8 μm), graphite (average particle size 80 μm), solvents and dispersants were mixed to achieve a dispersed suspension. In the second stage, a binder and plasticizer were added to the suspension and mixed further. Mixing was done by ball mill for 12 h. The composition of suspension and function of the additives are shown in Table 1. The mixed suspension was then deaired for 3 min under vacuum and cast into a tape to obtain a dry thickness ranging from 0.5 to 0.8mm. The dried tapes were then laminated together in a die at room temperature using a pressure of 75 MPa. These green compacts were then heated in air to remove the organic compounds and graphite contained in the tapes. This binder-removed step was done at a controlled heating rate to prevent blistering or cracking caused by emitted gases. Following burnout, the samples were presintered in an air atmosphere at 1280 °C for 2 h.

Table 1
Composition of suspension and function of the additives

Ingredient	Function	Volume percentage in suspension
ZrO_2	Ceramic powder	5–15
Graphite	Pore-forming agent	10–0
Ethanol absolute	Solvent	25
Acetone	Solvent	35
Triethyl phosphate	Dispersant	2.8
Polyvinyl butyral	Binder	7.2
Polyethylene glycol	Plasticizer	12.5
Diethyl-*o*-phthalate	Plasticizer	3.5

Three kinds of liquid precursors were synthesized by dilute phosphoric acid with cerium chloride. The synthetic method was as follows. Three kinds of solutions of $CeCl_3$ (0.05, 0.08 and 0.11mol/l) were rapidly added to dilute H_3PO_4 solution (P/Ce mole ratio 20) and magnetically stirred, respectively. The pH values of the mixing solutions were adjusted to about 1.0 by adding H_3PO_4 or ammonium phosphate solution. Several physical properties of the liquid precursor of various consistencies are summarized in Table 2. The viscosity of the liquid precursors at 25 °C was obtained using a rotation viscometer. The presintered porous zirconia made by adding graphite 30 vol.%, contained within a chamber, was evacuated of gas by a mechanical vacuum pump, then the liquid precursor was introduced into the chamber to cover the specimen. The specimen was covered with the precursor for an infiltration period of 8 h to ensure complete infiltration. When the specimen was removed from the chamber a layer of precursor clung to the specimen. The dried layer of precursor was removed with SiC paper prior to pyrolysis. The infiltrated specimen was heat-treated at 1000 °C for 2 h. Repeated infiltration and pyrolysis were performed using the same procedures. After different infiltration/pyrolysis cycles, the samples were isostatic hot-pressed for 2 h at 1600 °C in air to get greater than 98.5% of their theoretical densities.

The bulk density (including open and closed porosity) and apparent density (including only closed porosity) of the presintered pieces and the relative density of the

Table 2
Physicochemical properties of liquid precursors

No.	Viscosity (Pa s) at 25 °C	Ceramic yield (wt.%)	Composition after pyrolysis	pH
A	0.15	30	$CePO_4$	1.0
B	0.20	35	$CePO_4$	1.2
C	0.25	40	$CePO_4$	1.1

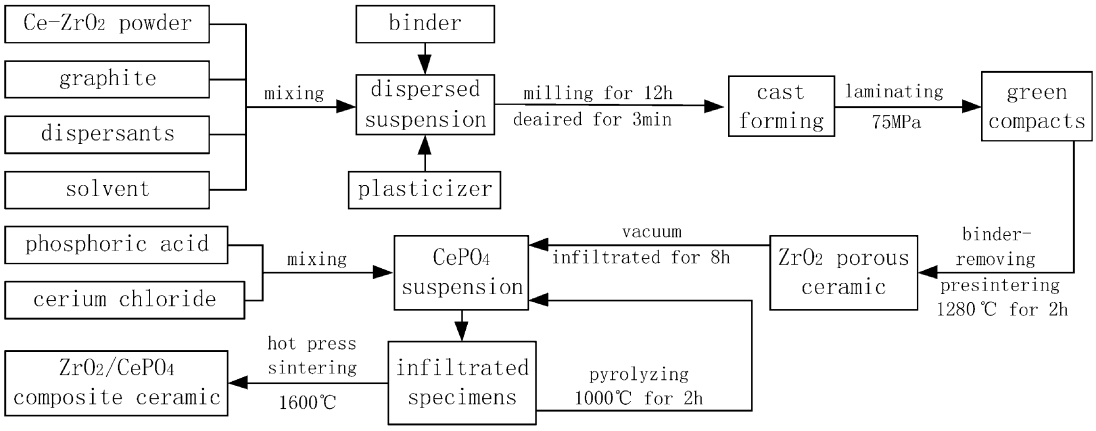

Fig. 1. Experimental procedure for preparation of Ce–TZP/$CePO_4$ composite ceramics.

sintered pieces were measured using a xylene vacuum penetration technique in combination with the Archimedes method. The volume ratio of $CePO_4/ZrO_2$ against the infiltration cycles was calculated from the atomic weight ratio of Ce/Zr examined by energy-dispersive X-ray spectroscopy (EDS), assuming that both phases were stoichiometric with a density of 6.26 g/cm^3 for Ce–TZP and 5.20g/cm^3 for $CePO_4$. Fracture surfaces of presintered pieces and the microstructure of the $CePO_4$ phase dispersing in hot-pressed zirconia matrix were examined by scanning electron microscopy (SEM).

The bending strength of the Ce–TZP/$CePO_4$ composite ceramics was measured with diamond-machined bar specimens (0.3×0.3×2.5 cm) using a three-point flexural test (span 2.0 cm) in mechanical testing machine, the tensile surfaces of the specimens were polished to a 1 μm finish with diamond paste, and the edges were beveled to remove damage introduced during diamond machining. The plane strain fracture toughness (K_{IC}) was determined by using a single-edge-beam (SEPB) method, precracked by the bridge-indentation technique. Beam specimens were ground flat and parallel to each opposite face with a 400 grit diamond wheel to obtain rectangular beams of dimensions 0.3×0.4×2.0 cm. The hardnesses of the materials were measured by using Vickers indentation with 100 N load. Their Young's moduli were estimated from the rule-of-mixture for a two-phase material. The tetragonal ZrO_2 contents by volume present of total ZrO_2 were measured by X-ray diffraction (XRD) technique on the as-fired surfaces and on the fractured surfaces of isostatic hot-pressed specimens.

The machinability of the Ce–TZP/$CePO_4$ composite ceramics was tested by using a diamond grinding wheel as shown schematically in Fig. 2. The diamond grinding measurements were obtained by using a 180 grit, resin-bond wheel (15.24 cm diameter, 6 mm width) rotating at 3600 rpm on a standard surface grinding machine with a spray of the aqueous cutting fluid. Test specimens of uniform width (10 mm) and thickness (4 mm) were mounted in a row on the load cell, so that the grinding wheel passed over each specimen sequentially in a single pass, thereby ensuring common grinding condition for all of the materials. Measurements of the normal grinding force were obtained for 20 μm depths-of-cut using a constant translation speed of ~2.8 cm/s.

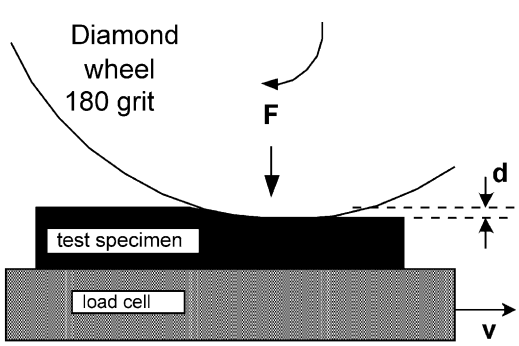

Fig. 2. Schematic diagrams illustrating the test setup for grinding measurements.

3. Results and discussion

3.1. Porosity and microstructure of the presintered zirconia porous ceramics

The effect of the volume of graphite on porosity can be demonstrated in Fig. 3. Clearly, all of the porosity which is closed below 10 vol.%, begin to open up at 15 vol.%, and, was completely open about 20 vol.%. The openness of porosity is a result of the contiguity of the graphite. Some residual closed porosity still remains in the presintered pieces. This closed porosity may be a result of unsintered zirconia powder. Mercury porosimetry is performed on the presintered ceramics. A typical porosimetry result is shown in Fig. 4 for the sample made by adding graphite 30 vol.%. It is obvious that the sample has a bimodal pore size distribution. A few small pores (2 μm) in the texture arise from the sintered necks between ZrO_2 particles. Fig. 5 showed the micrograph of the porous ceramic. Most of the pore sizes are in the range of 60–100 μm.

3.2. Effect of infiltration times on the $CePO_4$ content of the Ce–TZP/$CePO_4$ composite ceramics

The $CePO_4$ of the infiltrated and pyrolyzed bodies as a function of the number of infiltration cycles is shown in Fig. 6. As expected, the higher ceramic yield of the liquid precursor is more effective in increasing the $CePO_4$ content. However, attempts to increase the $CePO_4$ content with more infiltration cycles beyond a certain point are not successful. $CePO_4$ phase changes into a more discrete, particulate-like morphology after 1000 °C, the pore channels within presintered Ce–TZP

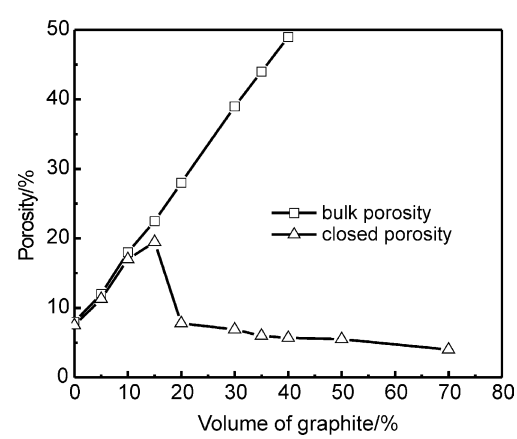

Fig. 3. Bulk and closed porosity versus the volume of graphite.

ceramics were severely restricted by the pyrolyzed precursor. The flow resistance of the materials became too large to allow intrusion of the viscous precursor. It could be seen that the change of $CePO_4$ content was smaller for subsequent cycles after the initial infiltration and pyrolysis steps. Infiltration and pyrolysis step produced a microstructure with smaller pore sizes, so the intrusion of liquid was less for a subsequent cycle than for the former cycle.

3.3. Mechanical properties of the Ce–TZP/$CePO_4$ composite ceramics

The hardnesses and Young's moduli of the Ce–TZP/$CePO_4$ composites were shown in Table 3. The softer $CePO_4$ phase dominated the hardness of the Ce–TZP/$CePO_4$ composite, which is 7.4∼6.2GPa over the composition range of 2.3∼10.5 vol.% $CePO_4$. The $CePO_4$ content dependence of the flexural strength and the fracture toughness of the Y–TZP/$CePO_4$ ceramics are presented in Fig. 7. The strength is relatively insensitive to $CePO_4$ content. However, the toughness is more strongly affected by the fractions of the two phases. Fig. 8 shows the tetragonal ZrO_2 contents determined by the XRD technique on as-fired surface and on fractured surfaces as a function of $CePO_4$ addition. As the restraining effect of the $CePO_4$ possessing softer hardness and lower Young's modulus decrease, at higher $CePO_4$ volume fraction, the tetragonal ZrO_2 content on the air-fired surface of the composite ceramics decreases with increasing $CePO_4$ content. When the $CePO_4$ is more than 7.5 vol.% the decrease in the fracture toughness is due to the spontaneous tetragonal-monoclinic transformation during cooling of the composites from the fabrication temperature and therefore a decrease in the amount of the available transformational tetragonal zirconia presents in the Ce–TZP/$CePO_4$ composites. The internal strains associated with the transformation are able to introduce microcracks in the composites. The microcracks will substantially reduce the fracture strength. Although the strength of samples decreases gradually with increasing $CePO_4$ content, the strength of sample containing $CePO_4$ 10.5 vol.% remains at 500 MPa. The result indicates that the critical flaws are not pores, which have been eliminated by being isostatic hot-pressed, and the critical flaws are a kind of surface flaw, whose size appears to be larger with increasing amount of $CePO_4$ between 2.3 and 10.3 vol.%.

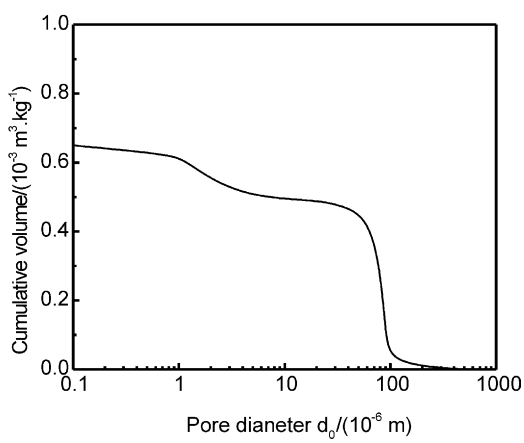

Fig. 4. Porosimetry for presintered sample made by adding graphite 30 vol.%.

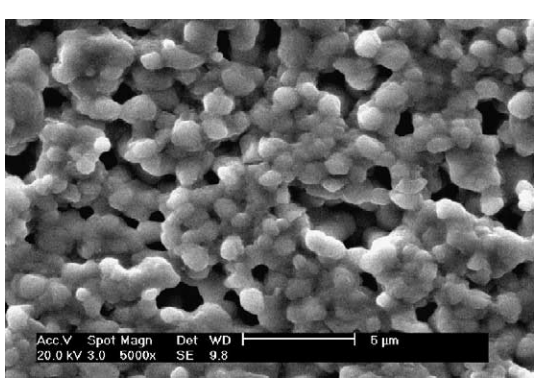

Fig. 5. SEM micrograph showing presintered porous ceramic.

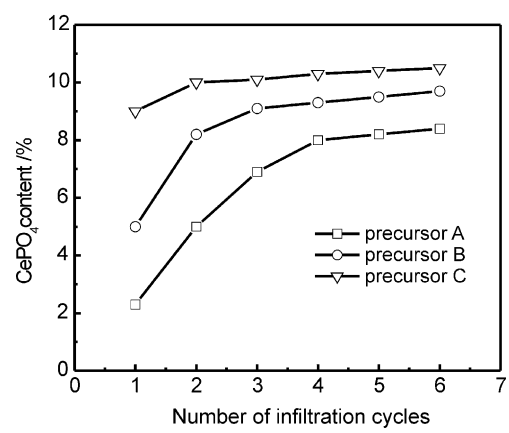

Fig. 6. $CePO_4$ contents versus number of cycles of infiltration for Ce–TZP/$CePO_4$ ceramics.

Table 3
Hardnesses and Young's moduli of Ce–TZP/$CePO_4$ composite ceramics

Ce–TZP/$CePO_4$ ($CePO_4$ content/vol%)	Hardness (GPa)	E (GPa)
0.0(Y–TZP)	9.50	200.0
2.3	7.40	198.4
5.2	7.05	196.5
7.1	6.75	195.2
8.3	6.50	194.4
9.2	6.34	193.7
10.0	6.22	193.2
10.3	6.20	193.0
100.0($CePO_4$)	5.40	132.0

3.4. Machinability of the Ce–TZP/$CePO_4$ composites ceramic

All of the composites can be drilled by tungsten carbide tool. Fig. 9 shows the normal grinding force as a function of the $CePO_4$ content of the Ce–TZP/$CePO_4$ ceramics. The results show that ease of diamond grinding is increased with the amount of $CePO_4$ content. The grinding force, P, for a given rate of material removal, is related to the microscopic hardness, H, fracture toughness, K_{IC}, and elastic modulus, E, of the material:[6]

$$P \propto \left[K_{IC}^{1/2} H^{5/8}/(E/H)^{4/5}\right]^{8/9} \quad (1)$$

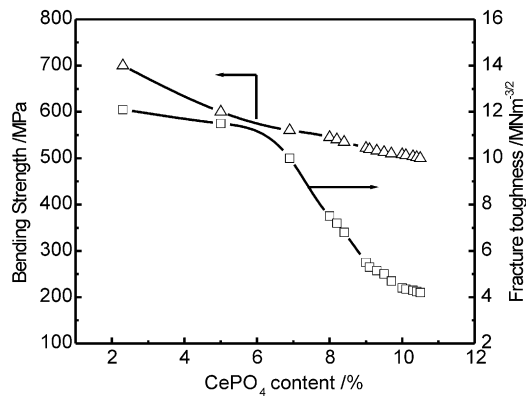

Fig. 7. Effect of $CePO_4$ content in Y–TZP on strength and toughness of Ce–TZP/$CePO_4$ composite ceramics.

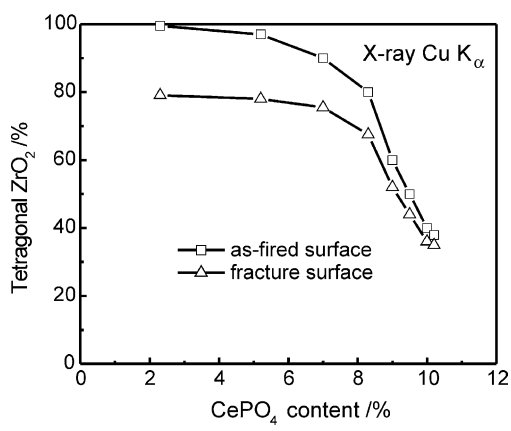

Fig. 8. Change of tetragonal ZrO_2 content on Ce–TZP/$CePO_4$ composite ceramics measured for as-fired and fracture surface.

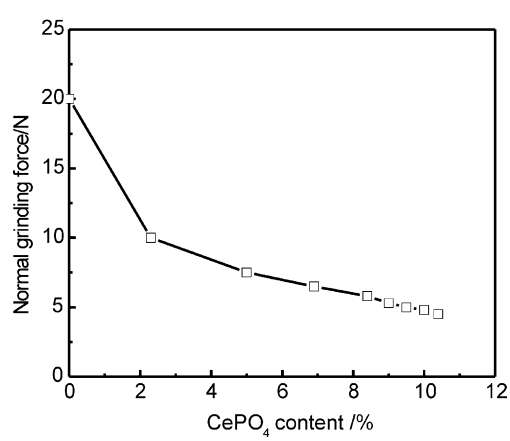

Fig. 9. The normal grinding force of Ce–TZP/$CePO_4$ composite ceramics.

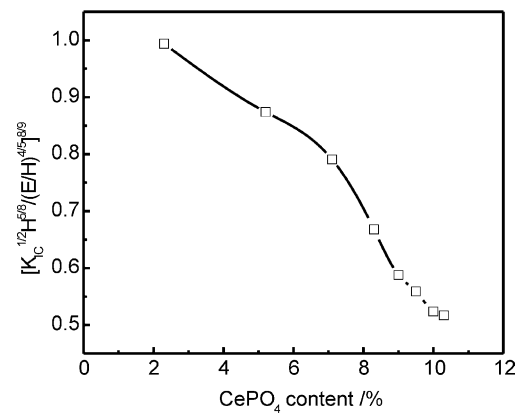

Fig. 10. $[K_{IC}^{1/2}H^{5/8}/(E/H)^{4/5}]^{8/9}$ of the composites versus $CePO_4$ content in the composite ceramics.

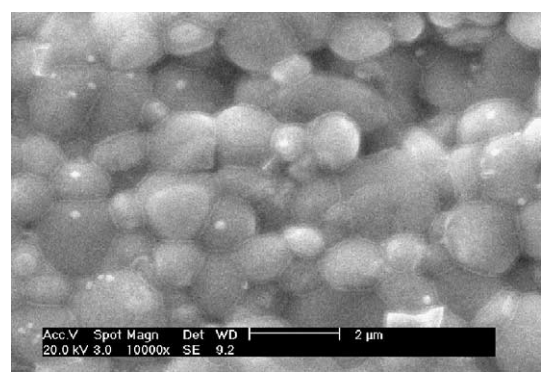

Fig. 11. SEM micrograph of Ce–TZP/$CePO_4$ sample containing $CePO_4$ 7.5 vol.%.

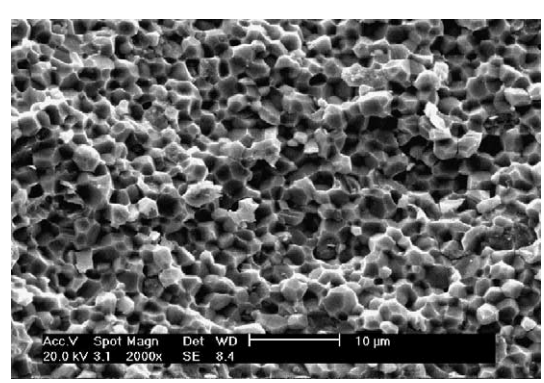

Fig. 12. SEM micrograph of fractured surface of Ce–TZP/$CePO_4$ sample containing $CePO_4$ 7.5 vol.%.

The $[K_{IC}^{1/2}H^{5/8}/(E/H)^{4/5}]^{8/9}$ of the composite, using measured values of H and E from Table 3 and values of K_{IC} for the composites measured by SEPB method, is plotted versus $CePO_4$ content in the composites in Fig. 10. The measured grinding forces for all of the materials of this study at 20 μm depth-of-out (in Fig. 9) are compared with Fig. 10. The result shows that the data mostly follow the trend predicted by Eq. (1). Easy material removal should occur by formation of cracks from a weak interface between the ZrO_2 and $CePO_4$ phases. The SEM micrograph of composite containing $CePO_4$ 7.5 vol.% is shown in Fig. 11. The bright regions around the ZrO_2 grains correspond to $CePO_4$. Intergranular $CePO_4$ second-phase has a beneficial effect in terms of inhibiting uneven grain growth and obtaining uniformity in grain size of ZrO_2. This microstructure has effectively improved the Ce–TZP ceramics' machinability as well as maintaining the outstanding mechanical properties. Fig. 12 shows the fractured surface of composite containing $CePO_4$ 7.5 vol.%. The microstructure shows little porosity, ZrO_2 grains in the size range of 2–3 μm, and intergranular fracture of grains.

4. Conclusion

1. Ce–TZP containing 2.3–10.5 vol.% $CePO_4$ was manufactured by liquid precursor infiltration. The Ce–TZP/$CePO_4$ composite ceramics develop a characteristic microstructure of uniformly small ZrO_2 grains with fine intergranular $CePO_4$ second-phases particles.
2. The attractive mechanical properties of the Ce–TZP/$CePO_4$ composites containing $CePO_4$ 2.3–7.5 vol.% are due to the high density of these composites and the high transformability of tetragonal zirconia in these composites.
3. The Ce–TZP/$CePO_4$ composites can be shaped with conventional WC metal-working tools. The ease of machining increased with increasing volume fraction of $CePO_4$ component. Microcracking at the interface between the two phases is involved in the mechanism of material removal.

Acknowledgements

The authors thank Professor Zhiguo Xiao and Xixian Luo for their useful suggestions and valuable discussions. This work was supported by National High Technology Research and Development Program of China under contract number 2002AA324060.

References

1. Chyung, K., Beall, G. H. and Grossman, D. G., Microstructures and mechanical properties of mica glass-ceramics. In *Proceedings of the 10th International Conference on Glass*, ed. G. Thomas. University of California, Berkeley, CA, 1974, pp. 1167–1194.
2. Barsoum, M. W. and Ei-eaghy, T., Synthesis and characterization of a remarkable ceramic: Ti_3SiC_2. *J. Am. Ceram. Soc.*, 1996, **79**, 1953–1956.
3. Padture, N. P., Evens, C. J., Xu, H. H. K. and Cewn, B. R., Enhanced machinability of silicon carbide via microstructure design. *J. Am. Ceram. Soc.*, 1995, **78**, 215–217.
4. Kawai, C. and Yamakawa, A., Machinability of high-strength porous silicon nitride ceramics. *J. Ceram. Soc. Jpn*, 1998, **106**, 1135–1137.
5. Davis, J. B., Marshall, D. B., Housley, R. M. and Morgan, P. E. D., Machinable ceramics containing rare-earth phosphates. *J. Am. Ceram. Soc.*, 1998, **81**, 2169–2175.
6. Evans, A. G. and Mashall, D. B., Wear mechanisms in ceramics. In *Fundamentals of fraction and wear of materials*, ed. D. A. Rigney. American Society of Mechanical Engineers, New York, 1981, pp. 439–441.